Radial head fractures: a quantitative analysis

Silvio Lampaert, Jan Herregodts, Lieven De Wilde, Alexander Van Tongel

From the Department of Orthopedics and Traumatology, University Hospital Ghent, Ghent, Belgium

Several classification systems for radial head fractures discuss the number of fragments and their displacement, but not the exact location. This study aimed to evaluate the location of the radial head fracture fragments and the influence of the Mason type on the size of the fracture fragment. Forty-one radial head fractures (31 Mason type I and 10 type II) with an elliptical radial head were included in this retrospective study and 3D reconstructed. First, the fragments were repositioned to their original location. Next, the orientation of the scanned forearm was evaluated using the position of the longest axis relative to the proximal radio-ulnar joint, and all radial heads were rotated to the neutral rotation. The radial head was divided into 4 quadrants (anteromedial, anterolateral, posteromedial, and posterolateral). The location of the fracture line in correlation with these 4 quadrants was evaluated. All fracture fragments were located in the anteromedial quadrant. Thirty-eight (93%) were located in the anterolateral quadrant. The posterolateral quadrant was involved in 32%. At last, the average fracture fragment size was evaluated according to the Mason classification. A significant difference was found in the average fracture fragment size between Mason type I (38% of the radial head surface) and type II (48% of the radial head surface). It was concluded that there is an important involvement of the anterior quadrants of the fracture. The mean size of the fracture is significantly larger in Mason type II compared to type I.

Keywords: radial head fracture; 3D CT reconstruction; forearm rotation; quantitative analysis; Mason classification; size fracture.

INTRODUCTION

A radial head fracture can occur with a fall on an extended arm. It is a frequent pathology with an incidence of 25 to 39 per 100,000 *(1)*. The fracture pattern depends on several factors: the vector of impact, the hand position, and rotation at the time of impact, firmness of the bones and the surrounding soft tissues *(2)*.

Classifications have been proposed to describe the radial head fracture. These classifications make it possible to compare the types of radial head fractures in an orderly arrangement of management and results *(3)*. The most commonly used classification is the Mason classification. Other classifications (Johnston, Broberg and Morrey, Hotchkiss…) have been developed to strive for a better intra- and inter-observation agreement *(1,4)*. However, the Mason classification or the other classifications do not describe the exact location of the fracture fragments. This knowledge may be helpful to have

■ Silvio Lampaert, MD,
■ Jan Herregodts, MD,
■ Lieven De Wilde, MD, PhD,
■ Alexander Van Tongel, MD, PhD.
Department of Orthopedics and Traumatology, University Hospital Ghent, Ghent, Belgium.
Correspondence : Silvio Lampaert, Medical doctor at University of Gent, Sint Pietersnieuwstraat 33, 9000 Gent, Belgium. Phone: +32/4 74 19 88 98.
Email : silviolampaert@gmail.com

a better understanding of the fracture mechanisms and to optimize the (surgical) treatment.

In several intra-articular fractures, the location of the fracture fragment has been evaluated using 3D CT scan images. This technique can also be used for the radial head, but, in contrast to other joints, the position of the scanned radial head is not standardized *(5,6)*. As a consequence, the fractured radial head can be scanned in pro- or supination. In most cases, only the proximal part of the elbow is scanned and not the complete forearm. This makes it difficult to measure the correct rotation of the scanned radial head. However, this knowledge is necessary to describe the location of the fracture fragments of the radial head in a standardized way. Deschrijver et al. described a new technique to calculate an elliptical radial head pro-supination position using the longest axis (LARH) and the proximal radio-ulnar joint (PRUJ) *(7)*.

The goal of this study was to define the location of the radial head fracture fragments using the technique described by Deschrijver et al. and to correlate the Mason type to the size of the fracture fragment.

MATERIALS AND METHODS

This retrospective study was approved by the ethical committee of the Ghent University Hospital (B670201733613). In total, 50 CT images of radial head fractures were investigated. These images were collected between January 2014 and January 2019.

The CT images were imported into Mimics 20.0.0® (Materialize, Leuven, Belgium). The radius, ulna, and humerus were 3D reconstructed. The radial head fractures were independently classified according to Mason by two authors (S. L., A. V. T.). If there was a difference in opinion concerning the classification, the fractures were reevaluated by both authors together, and a consensus was found. For this study, Mason type III fractures were excluded because no primary fracture line could be evaluated. All right elbows were mirrored in the left elbows to obtain standardization of the measurements. Each calculation was compared between the left and right elbow to ensure there was no significant difference.
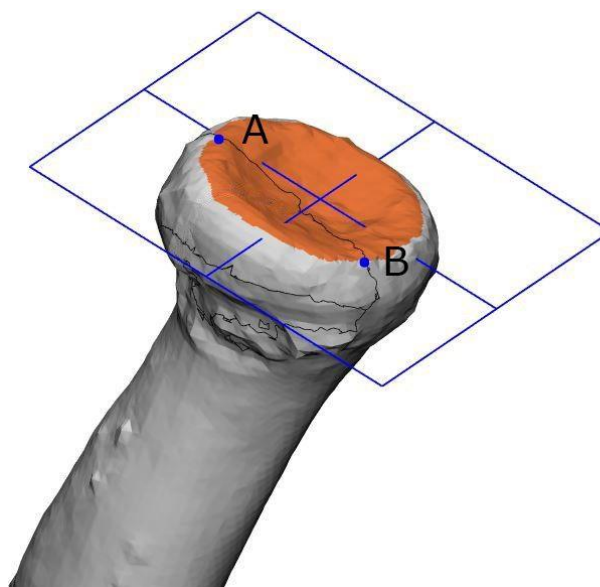

Figure 1. — The articulation plane with most medial (A) and most lateral (B) fracture points.

The segmented structures were exported to 3-Matic Research 11.0.0® (Materialize, Leuven, Belgium). The bone fragments were manually repositioned, and the radial head was reconstructed. Next, the proximal joint area of the radial head was marked, and the articulation plane of the radial head (RPlane), which is the best fitting plane, was automatically calculated. The most medial (A) and most lateral (B) fracture points were marked. (Figure 1)

After that, the rotational position of the forearm was determined according to the technique described by Deschrijver et al. *(7)*. To use this technique, the shape of the radial head (circular or elliptical) needs to be evaluated. If the radial head is circular, the technique described by Deschrijver et al. could not be used. The 2D CT scan in Mimics® was resliced using RPlane as reference. In the axial 2D CT images, the radial head was manually encircled. Subsequently, the longest axis (LARH) and shortest axis (SARH) were automatically calculated, with the center of the radial head (CR) defined as the intersection of both axes. (Figure 2) The shape of the radial head was evaluated by comparing the length of the LARH and SARH. Defined by G. Captier et al., the radial head is elliptical when the difference
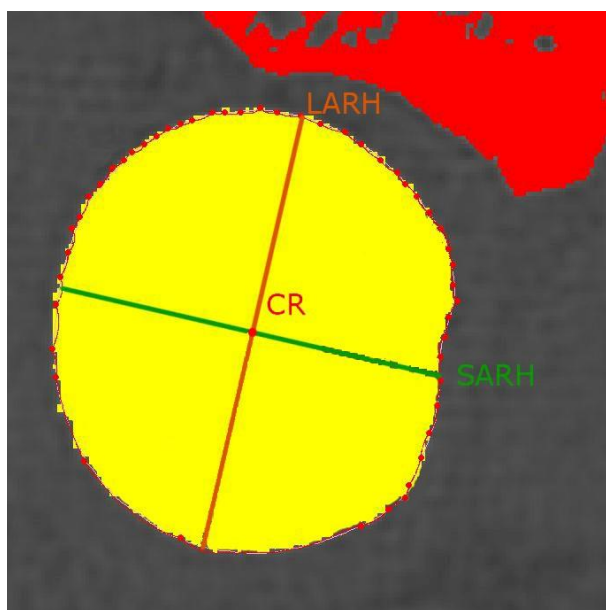
Figure 2. — The dotted line followed the outer contour of the radius. LARH and SARH were automatically calculated. The center of the radial head (CR) is the intersection of both axes.

between LARH and SARH is more than 1mm *(8)*.

The proximal radioulnar joint (PRUJ) plane was created using the anterior, posterior, and inferior points of the incisura radialis. The angulation between LARH and the PRUJ plane can be used to evaluate the orientation of the scanned forearm. Deschrijver et al. discovered the radius is located in 33° pronation (SD 14°) when LARH is perpendicular to PRUJ *(7)*.

The radius was rotated according to the RPlane to neutral rotation by two maneuvers. The first step was to rotate the radial head until the angle between the LARH and the PRUJ was perpendicular. The second step was the supination of 33°, which resulted in a neutral rotation of the radial head. Using the neutral rotation of the radius allows us to compare this study with others *(6,9)*.

The fracture fragment was defined as the fractured part that was not attached to the radial neck. The location of the fracture was analyzed using Photoshop CS 6®. The fracture in the top view of the joint surface was visualized. The radius was divided into 4 parts, starting from the anterior point (P_{SARH}): anteromedial, anterolateral, posteromedial, posterolateral and 12 segments (0°-30°, 30°-60°, -
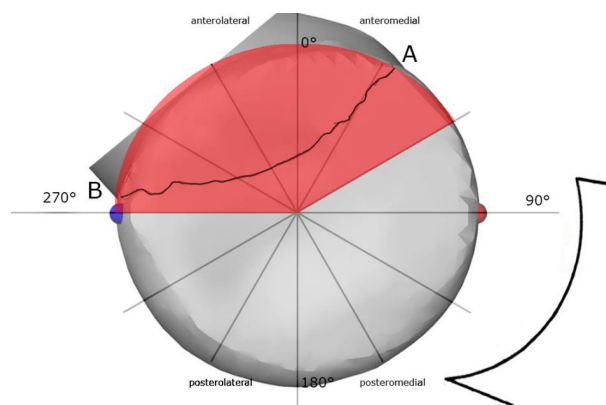

Figure 3. — The reconstructed radial is in a neutral position. PSARH is located at 0 degrees. The fracture line passes through the different segments, which are highlighted in red, with A the most medial point and B the most lateral point.

60-90°, ….330°-360°). P_{SARH} was the intersection of the radial contour and SARH. (Figure 3) Afterwards, the most medial (A) and the most lateral (B) points were highlighted. This visualization was based on Van Leeuwen et al. *(9)*.

In the reconstructed radial head, the location of the fracture fragment was defined by the segments that were passed by the fracture fragments from the medial fracture point (A) to the lateral fracture (B) point. (Figure 3)

Because Deschrijver et al. described a standard deviation of 14° when using the LARH, the radial head was rotated in an extra 14° of supination and an extra 14° of pronation. The location in these two new positions was also evaluated, aiming to be more accurate with the location of the fracture fragment. Points A en B were noted, as seen in table I. In table II and III the fracture points were noted for the correction of the standard deviation.

To calculate the ratio of the fracture fragment to the total area, a top view of the reduced radial head was created with the entire joint surface visible. Photoshop CS 6® (Adobe Systems Incorporated, San José, America) was used. (Figure 4) All pixels in the image were automatically selected. The pixels of the non-displaced radial head and the total area were calculated to obtain the relative area of the fracture fragment.

The normality test evaluated the distribution of the fractured area for Mason type I and II. According
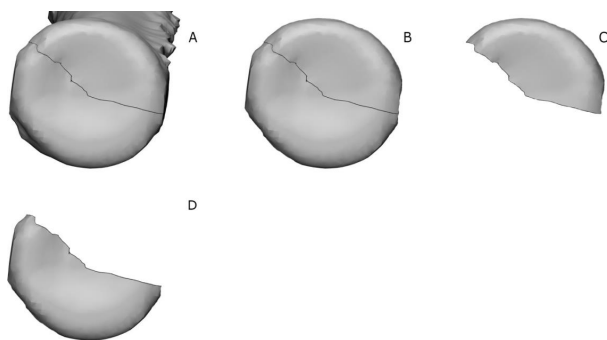
Figure 4. — Top view of the radius head (A), the joint area (B) and the area of the fracture (C), and the non-displaced radial head (D).

to the Mason classification, an independent T-test was performed to ascertain a significant difference in the area of the fracture.

Each elbow was reconstructed twice. The statistical analysis of the radial head was performed using SPSS® Statistics 26. To confirm the definition of G. Captier et al., a paired student t-test was performed *(8)*. The intra-class correlation (two-way random and absolute agreement) was used to determine the correspondence between the two reconstructions.

RESULTS

50 Radial head fractures were 3D reconstructed. Three patients were found to have a type III Mason through which they were excluded. Six patients had a difference between the LARH and SARH less than 1mm and were considered as a non-elliptical radial head. The ICC for LARH with Mason type I was 0.94. The value for Mason type II was similar. Forty-one patients had an elliptical radial head, and the technique of Deschrijver et al. could be used. The ICC of the position of the elbow was scanned, corresponded to 0.97 for type I and 0.88 for type II.

There was no significant difference (p > 0.05) between calculations performed at the left and right elbow. This allowed mirroring the radial head for standardization.

All the radial head fractures were located in the anteromedial quadrant. Thirty-eight (93%) were located in the anterolateral quadrant. The posterolateral quadrant was involved in 32%. (Figure 5) If the standard deviation is taken into account,

there was no difference in the evolvement of the anteromedial quadrant. The fracture was located less than 60% in the posterolateral quadrant (22% (+14°) and 51% (-14°)).

The distribution of point A (most medial) and B (most lateral) of the radial head fracture is found in Tables I, II, and III. (Figure 3) This data was divided according to the Mason classification. There was a similar distribution between the different Mason types.

The distribution of the fractured area was evaluated for Mason type I and II by the normality test, which showed a normal distribution. The average size of the fracture for Mason type II was 48%, and for Mason type I 38%. (Table IV) This was significantly different (p 0.04).

DISCUSSION

Several studies evaluated the number of fragments of radial head fractures and their displacement. Still, only a few studies have described the location of the fracture line in radial head fractures *(6,8,9)*.

Van Leeuwen et al. and Mellema et al. described that the anterolateral quadrant is the fracture's most common location *(6,9)*. In the study of Van Leeuwen et al., the anteromedial quadrant was involved in 79% of the fractures and the posterolateral in 77%. Also, Couture et al. described the location of the fracture line. However, they did not divide the radial head into 4 quadrants, but they evaluated the location of the fracture line compared to the safe zone *(10)*.

In our study, a ratio of 100% for the anteromedial and 32% for the posterolateral quadrant was found. (Figure 5) Also, if the standard deviation is taken into account, the fracture is still located less than 60% in the posterolateral quadrant (23% (+14°) and 55% (-14°)) and always anteromedial. (Figure 5)

A possible reason for the different results in our study compared with the other studies is the different measurement techniques to evaluate the rotation of the scanned forearm. First, all three other authors used the most prominent point of the tuberositas radii as the "zero-axis" in their Cartesian coordinate system and described the arm in a neutral position, when the tuberosity was at 132° clockwise

Table I. — Point A and B of the fracture is noted for each radial head fracture classified according to Mason

Mason type	Point A			Point B		
	30° - 120°	60° - 120°	90° - 120°	240° - 270°	240° - 300°	240° - 330°
I	87%	61%	13%	19%	71%	84%
II	100%	70%	30%	20%	40%	80%
All combined	91%	65%	16%	20%	63%	82%

Table II. — Point A and B of the fracture is noted for each radial head fracture classified according to Mason corrected with + 14° standard deviation

Mason type	Point A			Point B		
	30° - 120°	60° - 120°	90° - 120°	240° - 270°	240° - 300°	240° - 330°
I	90%	68%	32%	16%	55%	84%
II	100%	90%	60%	10%	30%	80%
All combined	93%	73%	39%	15%	49%	83%

Table III. — Point A and B of the fracture is noted for each radial head fracture classified according to Mason corrected with - 14° standard deviation

Mason type	Point A			Point B		
	30° - 120°	60° - 120°	90° - 120°	240° - 270°	240° - 300°	240° - 330°
I	77%	42%	10%	35%	71%	77%
II	90%	60%	0%	30%	80%	80%
All combined	80%	46%	7%	34%	73%	78%

Table IV. — Descriptive statistics of the area of the fracture

	Mason type	N	Mean	Std. Deviation	Std. Error Mean
Area of the fracture	I	31	,3827	,1196	,0215
	II	10	,4779	,1292	,0408

(6,9,10). However, they did not include the SD of 8°, described by Hutchinsons et al. (11). We included the SD of 14° described by Deschrijver et al. (7). Next, they also assumed the maximum supination is 85°. The value for maximum supination is not universally accepted because it depends on the number of degrees of flexion in which the arm is scanned (12,13). At last, this technique is not always possible. Due to radiation exposure, the scanned region is always kept as small as possible. Therefore, the reference point, the tuberositas radii, is not always scanned.

The method based on Van Riet et al. does not depend on the tuberositas radii. Van Riet et al. found, based on empiric observation, the radial head is in the neutral rotation when LARH is perpendicular to PRUJ (5). This conclusion was invalidated by Deschrijver et al. They determined
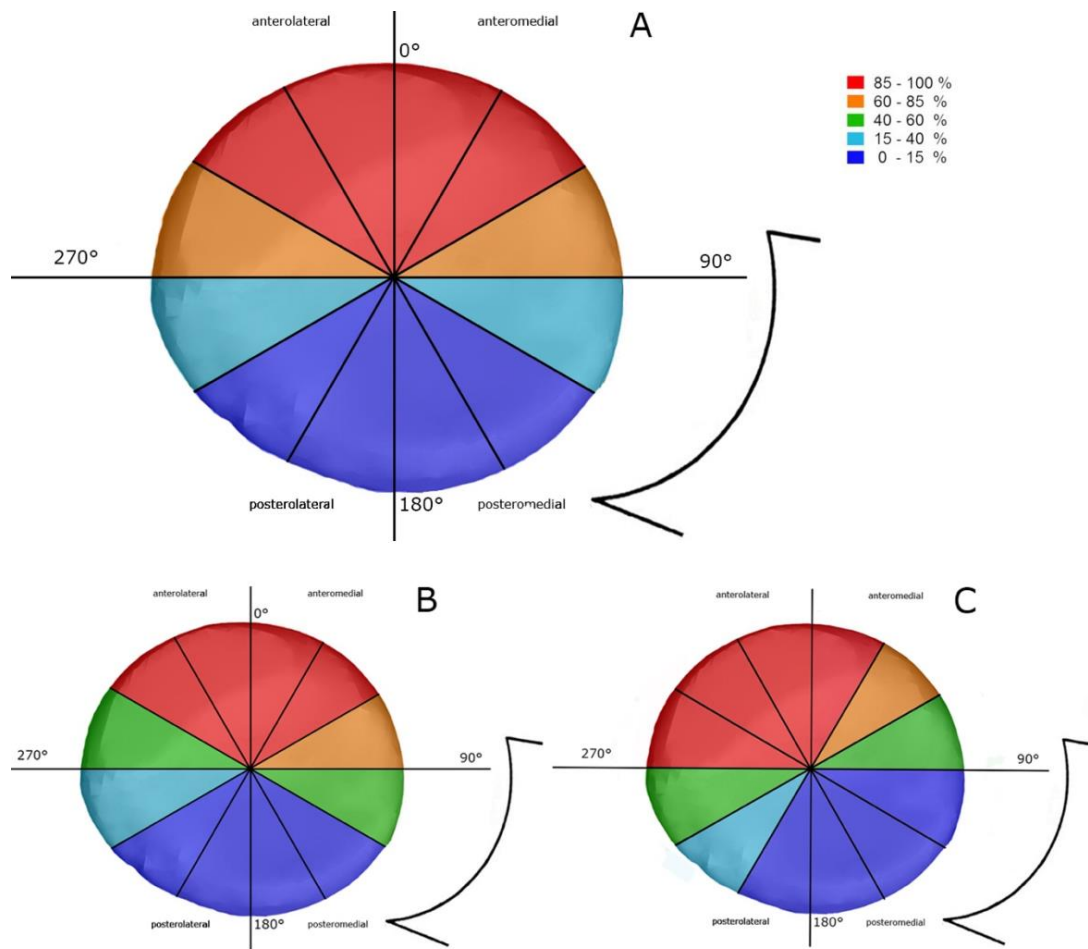
Figure 5. — Radius is in a neutral position and divided into four quadrants.
(A) The radius was rotated according to the standard deviation in B (14° pronation) and C (14° supination).

with a statistical analysis that the radial head is not in a neutral position but in 33° pronation (SD 14°) when LARH is perpendicular to the PRUJ *(7)*. The data from Deschrijver et al. was used to calculate the position the radial head was scanned. This technique applied to the 3D models shows a high ICC for each determination.

Our results showed that in the neutral forearm position, the fracture fragment is anterior. As a clinical consequence, if a lateral approach is used, the forearm needs to be brought in supination to get the fracture fragment lateral and to be able to put a screw perpendicular on the fracture line from lateral to medial.

If we hypotheses that a Mason type I and type II radial head fracture occurs because of the impact of

the radial head on the capitellum while the elbow (sub)luxate posterolateral, we can assume that, at the time of impact, the radius is most commonly in neutral rotation and not in complete supination or pronation. (Figure 5)

A possible explanation of our findings can be transposed in the biomechanical theory of O'Driscoll *(12)*. As with posterolateral rotatory instability, radial head fractures typically occur as a result of a fall on the outstretched arm with the elbow initially in the extended position. As an axial load is applied to the arm, the elbow sustains a valgus moment, and the distal rotates internally against the forearm that is fixed to the ground. This combination of axial load, valgus force, and rotation can result in disruption of the lateral collateral ligament. This ligamentous

disruption will allow the radial head to translate posteriorly to the capitellum. This is illustrated because the fracture is always C-curved as if the equator of the capitellum acted as a wedge to split the radial head and because the fractured part is found in the anterior part of the radial head. When evaluating our results, we can suggest, at the time of impact, the forearm is in neutral rotation.

When evaluating the distribution of the fracture line in Mason type I and type II, there is no clear difference. But there was a significant difference between the size of the fracture in type I and type II. The flexion of the elbow could explain the difference in fracture area at the time of impact. In Mason type II, this may be greater than in Mason type I. This will result in more contact with the capitellum, which explains the bigger area of the broken part of the radial head in Mason type II fractures. This hypothesis needs to be evaluated in a biomechanical lab.

Another clinical consequence of this study is the fact that, because in type II fracture, the average size of the fracture is larger, an extra screw can be used to stabilize the fracture if necessary.

A weakness of our study is the fact that the measurement technique could only be used in an elliptical radial head. This has two consequences. First of all, a few fractures could not take into account because they did have a circular shape. Secondly, reconstructing the radial head could impair the elliptical shape, and this could lead to a shift of the angle between PRUJ and LARH.

CONCLUSION

The goal of this study was to describe the location and the average size of the fracture in elliptical radial heads as this could explain the fracture mechanism and could have an impact on the reduction technique.

Compared with previous studies, a slightly different distribution of the radial head fracture is seen. In 93% of the cases, the anterolateral quadrant is involved and 100%, the anteromedial. The posterior quadrant is less involved.

There is no difference in distribution of the fracture line between Mason type I or Type II, but the average area is significantly greater for Mason type II compared to type I.

REFERENCES

1. Duckworth AD, McQueen MM and Ring D. Fractures of the radial head. Bone Joint J 2013;95-B:151-159. 2013/02/01.
2. Sheehan SE, Dyer GS, Sodickson AD, et al. Traumatic elbow injuries: what the orthopedic surgeon wants to know. Radiographics 2013;33:869-888.2013/05/16.
3. Little KJ. Elbow fractures and dislocations. Orthop Clin North Am 2014;45:327-340.2014/07/01.
4. Iannuzzi NP and Leopold SS. In brief: the Mason classification of radial head fractures. Clin Orthop Relat Res 2012;470:1799-1802. 2012/03/20.
5. van Riet RP, Van Glabbeek F, Neale PG, et al. The noncircular shape of the radial head. J Hand Surg Am 2003;28:972-978. 2003/12/04.
6. Mellema JJ, Eygendaal D, van Dijk CN, et al. Fracture mapping of displaced partial articular fractures of the radial head. J Shoulder Elbow Surg 2016;25:1509-1516. 2016/04/08.
7. Miguel Deschrijver SL, Guillaume Planckaert, Hannes Vermue, Lieven De Wilde, Alexander Van Tongel. Positioning of longest axis of the radial head in neutral forearm rotation Sage Journals 2019.
8. Captier G, Canovas F, Mercier N, et al. Biometry of the radial head: biomechanical implications in pronation and supination. Surg Radiol Anat 2002;24:295-301. 2002/12/24.
9. van Leeuwen DH, Guitton TG, Lambers K, et al. Quantitative measurement of radial head fracture location. J Shoulder Elbow Surg 2012;21:1013-1017. 2011/11/11.
10. Couture A, Hebert-Davies J, Chapleau J, et al. Involvement of the proximal radial ulnar joint in partial radial head fractures: a novel three-dimensional computed tomography scan evaluation method. Shoulder & elbow 2019;11:121-128. 2019/04/03.
11. Hutchinson HL, Gloystein D and Gillespie M. Distal biceps tendon insertion: an anatomic study. J Shoulder Elbow Surg 2008;17:342-346. 2007/10/13.
12. Shaaban H, Pereira C, Williams R, et al. The effect of elbow position on the range of supination and pronation of the forearm. J Hand Surg Eur Vol 2008;33:3-8. 2008/03/12.
13. Fu E, Li G, Souer JS, et al. Elbow position affects distal radioulnar joint kinematics. J Hand Surg Am 2009;34:1261-1268. 2009/07/07.